Adjoint Sensitivity Computations for an Embedded-Boundary Cartesian Mesh Method and CAD Geometry

Marian Nemec[1] and Michael J. Aftosmis[2]

[1] ELORET Corp., Moffett Field, CA 94035, USA *mnemec@mail.arc.nasa.gov*
[2] NASA Ames Research Center, CA 94035, USA *maftosmis@mail.arc.nasa.gov*

Key words: shape optimization, adjoint, Cartesian mesh, cut-cells

1 Introduction

Complex geometry remains a challenging issue facing the application of adjoint and flow-sensitivity methods in practical engineering design. Among the most promising approaches for complex-geometry problems is the embedded-boundary Cartesian mesh method [1]. In this approach, the discretization of the surface geometry is decoupled from that of the volume mesh, which enables rapid and robust mesh generation, and ultimately, an automatic analysis of aerodynamic performance. The purpose of this work is to extend the automation and efficiency of Cartesian methods to the computation of aerodynamic sensitivities for shape optimization problems.

The most common way to account for the effect of boundary shape perturbations in the adjoint and flow-sensitivity formulations is via domain mapping approaches. In implementations on *body-fitted* structured or unstructured meshes, this involves the use of mesh-perturbation schemes. For local shape deformations, the extent of the mesh perturbations can be limited to just the boundary cells [2, 3, 4]. The approach we propose here for *non-body-fitted* Cartesian meshes is similar, but the boundary faces of the volume mesh maintain their Cartesian orientation as the surface evolves. This approach permits the computation of mesh sensitivities via a direct linearization of the boundary-cell geometric constructors of the mesh generator.

2 Discrete Adjoints and Flow Sensitivities

Our goal is to minimize a scalar objective function $\mathcal{J}$, such as drag, by adjusting a design variable X using gradient-based optimization. To compute the gradient, $\mathrm{d}\mathcal{J}/\mathrm{d}X$, we use a discrete formulation. Hence, a variation in X

influences the computational mesh $\boldsymbol{M}$ and the flow solution $\boldsymbol{Q}$, which satisfies the three-dimensional Euler equations of a perfect gas. The spatial discretization of the flow equations uses a cell-centered, second-order accurate finite volume method with a weak imposition of boundary conditions, resulting in a system of equations

$$\boldsymbol{R}(X, \boldsymbol{M}, \boldsymbol{Q}) = 0 \tag{1}$$

where $\boldsymbol{M}$ is an explicit function of the surface triangulation $\boldsymbol{T}$: $\boldsymbol{M} = f[\boldsymbol{T}(X)]$.

The gradient of the objective function $\mathcal{J}(X, \boldsymbol{M}, \boldsymbol{Q})$ is given by

$$\frac{\mathrm{d}\mathcal{J}}{\mathrm{d}X} = \frac{\partial \mathcal{J}}{\partial X} + \frac{\partial \mathcal{J}}{\partial \boldsymbol{M}} \underbrace{\frac{\partial \boldsymbol{M}}{\partial \boldsymbol{T}} \frac{\partial \boldsymbol{T}}{\partial X}}_{\mathrm{A}} + \frac{\partial \mathcal{J}}{\partial \boldsymbol{Q}} \frac{\mathrm{d}\boldsymbol{Q}}{\mathrm{d}X} \tag{2}$$

The evaluation of the term $\mathrm{d}\boldsymbol{Q}/\mathrm{d}X$, referred to as the flow sensitivities, is obtained by linearizing Eq. 1

$$\frac{\partial \boldsymbol{R}}{\partial \boldsymbol{Q}} \frac{\mathrm{d}\boldsymbol{Q}}{\mathrm{d}X} = - \left(\frac{\partial \boldsymbol{R}}{\partial X} + \frac{\partial \boldsymbol{R}}{\partial \boldsymbol{M}} \underbrace{\frac{\partial \boldsymbol{M}}{\partial \boldsymbol{T}} \frac{\partial \boldsymbol{T}}{\partial X}}_{\mathrm{B}} \right) \tag{3}$$

The adjoint equation is obtained by combining Eqs. 3 and 2 and defining the following intermediate problem

$$\frac{\partial \boldsymbol{R}}{\partial \boldsymbol{Q}}^{\mathrm{T}} \boldsymbol{\psi} = \frac{\partial \mathcal{J}}{\partial \boldsymbol{Q}}^{\mathrm{T}} \tag{4}$$

where the vector $\boldsymbol{\psi}$ represents the adjoint variables. Details of the solution method for Eqs. 3 and 4 are given in [5]. We focus on the evaluation of the terms A and B in Eqs. 2 and 3, which are discussed in the next section.

3 Shape Sensitivities

The flow equations are discretized on a multilevel Cartesian mesh. The mesh consists of regular Cartesian hexahedra everywhere, except for a layer of body-intersecting cells, or *cut-cells*, adjacent to the boundaries. An infinitesimal perturbation of the boundary shape affects only the cut-cells. Consequently, the mesh-sensitivity term $\partial \boldsymbol{M}/\partial \boldsymbol{T}$, which contains the linearization of the Cartesian-face areas and centroids, volume centroids and the wall normals and areas with respect to the surface triangulation, is non-zero in these cells. The crux in the evaluation of $\partial \boldsymbol{M}/\partial \boldsymbol{T}$ is the linearization of the geometric constructors that define the intersection points between the surface triangulation and the Cartesian hexahedra.

We explain the salient steps of the linearization using the example shown in Fig. 1, where a Cartesian hexahedron is split into two cut-cells by the surface triangulation. We require the linearization of the intersection points

that lie on Cartesian edges, e.g., point A, and also those that lie on triangle edges, e.g., point B. Focusing on point B, its location along the triangle edge V_0V_1 is given by

$$B = V_0 + s(V_1 - V_0) \tag{5}$$

where s denotes the distance fraction of the face location relative to the vertices V_0 and V_1. The linearization of this geometric constructor is given by

$$\frac{\partial B}{\partial X} = \frac{\partial V_0}{\partial X} + s(\frac{\partial V_1}{\partial X} - \frac{\partial V_0}{\partial X}) + (V_1 - V_0)\frac{\partial s}{\partial X} \tag{6}$$

A similar constructor is used for point A [6]. An example result of the linearization is shown in Fig. 1 for the position sensitivity of Cartesian face centroids. Note that the "motion" of the face centroids is constrained to the plane of the face. An advantage of this formulation is that the dependence of the mesh sensitivities $\partial \boldsymbol{M}/\partial \boldsymbol{T}$ on the surface triangulation ($\partial V_1/\partial X$ in Eq. 6 and the term $\partial \boldsymbol{T}/\partial X$ in Eq. 3) is determined on-the-fly for each instance of the surface geometry. Put another way, there is no requirement for a one-to-one triangle mapping as the surface geometry changes. This allows a flexible interface for geometry control based on tools such as computer-aided design (CAD).

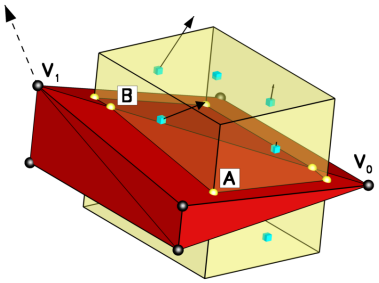

Fig. 1. Sensitivity of face centroids (solid vectors) to perturbation of vertex V_1.

4 Verification Studies

4.1 Supersonic Vortex Problem

We investigate the error convergence rate of a representative objective function and its gradient on a model problem with a known analytic solution [6]. The problem involves isentropic flow between concentric circular arcs at supersonic conditions, as shown in Fig. 2. The objective function is the integral of pressure along the outer arc, which is similar to the lift and drag objectives used in aerodynamic design. We compute the gradient and the sensitivities of the flow solution, Eq. 3, with respect to the inlet Mach number, M_i. The problem is solved on a sequence of five nested Cartesian meshes.

Figure 3 summarizes the results. Figure 3(a) shows the error convergence rates in the L_1 norm of density and its sensitivity to variations in M_i. The error convergence rate of the objective function

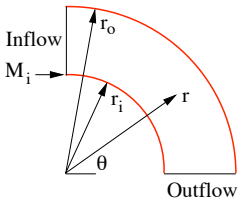

Fig. 2. Problem setup ($M_i = 2.25$, $r_i = 1$ and $r_o = 1.382$)

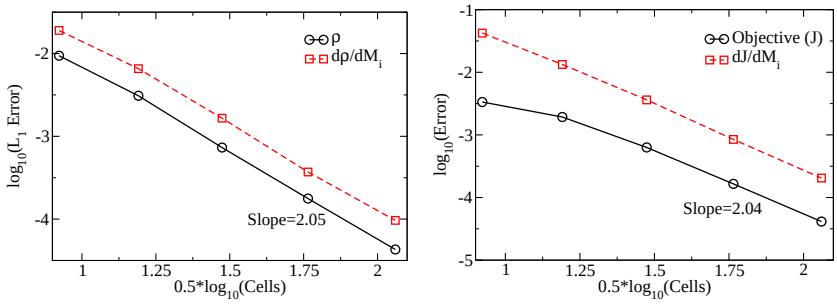

(a) Density and density gradient (b) Objective function and gradient

Fig. 3. Error convergence (slopes are computed using the three finest meshes)

and its gradient is shown in Fig. 3(b). The asymptotic convergence rate of all errors, which is measured over the three finest meshes, is just slightly over 2. These results verify the accuracy of the linearization and the convergence of these methods to the continuous problem.

4.2 Shape sensitivities for the NACA 0012 airfoil

The goal of this verification test is to study the convergence of gradients for design variables that alter the shape of the boundary. We consider a subsonic flow over the NACA 0012 airfoil at $M_\infty = 0.5$ and $\alpha = 1$ deg. We investigate the sensitivity of lift to the angle of attack using two equivalent approaches. First, we consider the influence of the angle of attack via a change in the farfield boundary conditions, which does not alter the relationship between the mesh and the airfoil. We contrast this with an angle of attack change implemented via a rigid-body rotation of the airfoil about its trailing edge within a fixed mesh. The mesh-refinement study is performed on a sequence of five nested Cartesian meshes for each airfoil orientation.

The results are summarized in Fig. 4. Referring to Fig. 4(b), note that the differences in the gradients between the farfield and rigid-body rotation cases are decreasing as the mesh is refined. Additional regression analysis of this data indicates that the rate of convergence is first-order. This is a consequence of the fact that the mesh perturbations are confined to only the cut-cells. Unlike the supersonic vortex problem, a perturbation of the angle of attack via rigid-body rotation modifies the cut-cell boundary and introduces an error in the objective function proportional to second-order spatial discretization. Nevertheless, the gradient values for the rigid-body rotation case, even on the coarsest mesh of roughly $3,200$ cells, are within 1% of the fine-mesh values.

5 Design Example: Reentry Capsule

We consider the optimization of a heat-shield shape for a reentry capsule. The objective is to enhance the lift-to-drag ratio, L/D, of the capsule, thereby im-

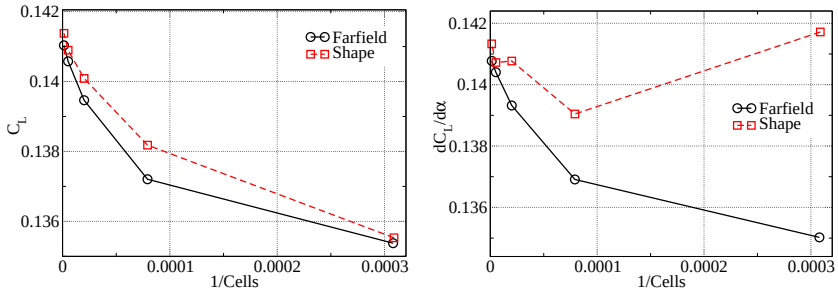

(a) Lift (b) Gradient of lift

Fig. 4. Convergence of lift and its gradient with respect to angle of attack: implemented via the farfield boundary ("Farfield") and rigid-body rotation ("Shape")

proving trajectory control for landing-site selection, and reducing the reentry load factor and heat rates. The Pro/ENGINEER® Wildfire CAD system is used to create the geometry model. The capsule configuration is shown in Fig. 5(a), where the design variables are the three labeled spline points of the heat-shield center-line. The freestream conditions are $M_\infty = 10$ and $\alpha = 156.5$ deg., measured clockwise from the positive x-axis. High-temperature effects are approximated by the use of an "effective" ratio of specific heats, γ. We use $\gamma = 1.3$. The initial (symmetric) capsule generates an L/D of 0.37, which is attained using a center-of-gravity offset. The target value of L/D is set to 0.4. The volume mesh contains roughly $665,000$ cells and we use 64 processors to solve the flow and adjoint equations.

Convergence of the optimization problem is shown in Fig. 5(b). The target L/D is reached within five design iterations and the L_2 norm of the gradient is reduced by roughly four orders of magnitude. The initial and final heat-shield shapes are shown in Figs. 5(c) and 5(d), respectively. The shape modifications are relatively minor, yet the improvement in L/D is 8%. The wall-clock time per design iteration is approximately 11 minutes. This time includes the regeneration and triangulation of the part, as well as the flow solution and adjoint gradient computation. We emphasize that for problems with more design variables, the design-cycle time would remain essentially constant.

6 Conclusions

We have presented an approach for the computation of aerodynamic shape sensitivities using a discrete formulation on Cartesian meshes with cut-cells at the wall boundaries. The verification studies show that the convergence rate of gradients is second-order for design variables that do not alter the boundary shape, and is reduced to first-order for shape design variables. This is a consequence of confining the mesh sensitivities to the cut-cells. The design example demonstrates the effectiveness of the new approach for engineering design studies that require a fast turn-around and include CAD-based geometry, complex flow, and many design variables.

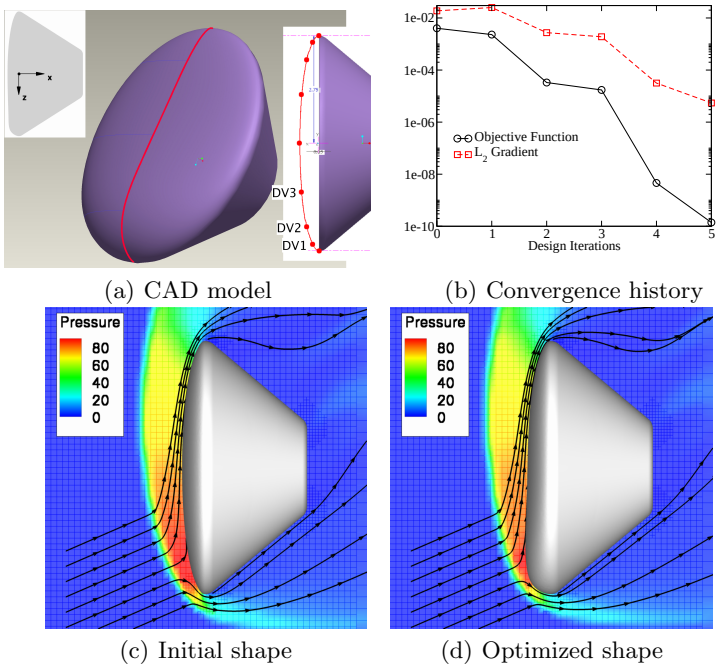

(a) CAD model (b) Convergence history

(c) Initial shape (d) Optimized shape

Fig. 5. Heat-shield shape optimization ($M_\infty = 10$, $\alpha = 156.5°$, $\gamma = 1.3$)

7 Acknowledgments

The authors gratefully acknowledge Robert Haimes (MIT) for help with CAPRI. This work was supported by the NASA Ames Research Center contract NNA05BF35C.

References

1. Aftosmis, M. J., Berger, M. J., and Melton, J. E., "Robust and Efficient Cartesian Mesh Generation for Component-Based Geometry," *AIAA Journal*, Vol. 36, No. 6, 1998, pp. 952–960.
2. Anderson, W. K. and Venkatakrishnan, V., "Aerodynamic Design Optimization on Unstructured Grids with a Continuous Adjoint Formulation," *Computers & Fluids*, Vol. 28, 1999, pp. 443–480.
3. Dadone, A. and Grossman, B., "Efficient Fluid Dynamic Design Optimization Using Cartesian Grids," AIAA Paper 2003–3959, Orlando, FL, June 2003.
4. Lu, J., *An* a posteriori *Error Control Framework for Adaptive Precision Optimization using Discontinuous Galerkin Finite Element Method*, Ph.D. thesis, Massachusetts Institute of Technology, 2005.
5. Nemec, M., Aftosmis, M. J., Murman, S. M., and Pulliam, T. H., "Adjoint Formulation for an Embedded-Boundary Cartesian Method," AIAA Paper 2005–0877, Reno, NV, Jan. 2005.
6. Nemec, M. and Aftosmis, M. J., "Aerodynamic Shape Optimization Using a Cartesian Adjoint Method and CAD Geometry," AIAA Paper 2006–3456, San Francisco, CA, June 2006.